Preprint
UCRL-JC-146831

Environmental Considerations in the Studies of Corrosion Resistant Alloys for High-Level Radioactive Waste Containment

G.O. Ilevbare, T. Lian, J.C. Farmer

This article was submitted to
National Association of Corrosion Engineers Corrosion Expo 2002,
Denver, CO, April 7-12, 2002

January 15, 2002

U.S. Department of Energy
Lawrence
Livermore
National
Laboratory

ENVIRONMENTAL CONSIDERATIONS IN THE STUDIES OF CORROSION RESISTANT ALLOYS FOR HIGH-LEVEL RADIOACTIVE WASTE CONTAINMENT

G.O. Ilevbare, T. Lian and J.C. Farmer

Lawrence Livermore National Laboratory
Livermore California 94550

ABSTRACT

The corrosion resistance of Alloy 22 (UNS No.: N06022) was studied in simulated ground water of different pH values and ionic contents at various temperatures. Potentiodynamic polarization techniques were used to study the electrochemical behavior and measure the critical potentials in the various systems. Alloy 22 was found to be resistant to localized corrosion in the simulated ground waters tested.

Keywords: Alloy 22, corrosion resistance, electrochemical behavior, open circuit potential (OCP), oxygen evolution potential, cyclic polarization, simulated acidified water (SAW), simulated concentrated water (SCW), J-13 water, Yucca Mountain, nuclear waste.

INTRODUCTION

The environmental considerations of importance here are those pertaining to the design and construction of high-level radioactive waste packages for the Yucca Mountain Project. As stipulated in the License Design Selection Report [1], the design of the waste package calls for a double walled canister (Figure 1). The proposed material for the outer barrier of the waste package is Alloy 22 (Unified Numbering System (UNS) N06022), the corrosion resistant material (CRM). This material is expected to provide a reasonable level of "kinetic" immunity from general and localized corrosion for the waste packages under the prevailing environmental condition in Yucca Mountain so that there is a low rate of passive dissolution, and negligible chance of stabilization of localized corrosion for periods of time in excess of 10,000 years. The proposed material for the inner barrier of the waste package is stainless steel 316 (UNS S31603). The primary role of this layer is structural reinforcement.

The composition of the ground water (well water) found at Yucca Mountain is described in Table 1. It is referred to as J-13 [2-4]. The water is so named because it was drawn from a well designated J-13 in the Nevada test site, located near Yucca Mountain. The well draws from the same rock unit as Yucca Mountain. J-13 is relatively benign to Alloy 22 for electrochemical testing especially over short periods of time [5, 6]. For this reason, the test media used for investigations are simulated ground waters derived for the continuous cyclic wetting and drying process (evaporative concentration) of J-13 expected under waste storage material conditions due to the heat anticipated from the radioactive decay of the waste material, and the constant dripping of the ground water onto the containers from pores in the surrounding rock [4]. However, this process is expected to occur after a significant drop in temperature as the heat generated initially is expected to keep the repository in a fairly dry state [7, 8]. Researchers at the Lawrence Livermore National Laboratory (LLNL) prepared several versions of the simulated waters, concentrated to over 1000 times of J-13 in the acidic, near neutral and basic regimes for realistic electrochemical testing [3]. They include Simulated Acidified Water (SAW), with a pH of ~ 2.8, Simulated Concentrated Water (SCW) with a pH of ~8, and Basic Saturated Water (BSW) with a pH of ~13.

Compared with other nickel (Ni) alloys, relatively little experimental data on corrosion exist on Alloy 22 because it is an alloy that is relatively new (~20 years old) [9]. The effects of temperature (25 to 200 °C) and electrolyte composition (0.017 M chloride concentration ($[Cl^-]$) to saturation) on the critical breakdown potentials for localized corrosion have been studied extensively on Ni alloys [10-22]. These studies show that an increase in temperature and $[Cl^-]$ reduces the critical breakdown potential while an increase in concentration of alloying elements like tungsten (W), chromium (Cr) and molybdenum (Mo) increases these breakdown potentials. The synergy between Cr and Mo in resisting localized corrosion is particularly potent. Alloy 22 is more resistant to localized breakdown, and exhibits much lower corrosion rates compared with alloys such as 625 and 825 [12-14, 19, 24-27]. Thus, in the context of chemistry change models of localized corrosion stabilization, a more severe environment is required to initiate breakdown in Alloy 22 compared with a less resistant alloy such as Alloy 625.

The ground water found in Yucca Mountain, and simulated ground waters used for experimentation in this work contain a diverse mixture of oxyanions. This undoubtedly makes the water chemistry, and the possible surface interactions of these various species with the metal surface complicated. Some of these oxyanions (e.g., nitrate (NO_3^-), sulfate (SO_4^{2-})) have been implicated in inhibiting localized corrosion in stainless steels and nickel [28-38]. Since the simulated waters (Table 1) contain an appreciable concentration of these oxyanions compared with Cl^-, it is expected that they will play a role in determining the critical potential for the onset of localized corrosion on Alloy 22. The effectiveness of inhibiting species has been found to depend on the ratio of concentration of the oxyanions (inhibiting species) to the aggressive species (e.g., Cl^-) in solution [28-38]. Below their various threshold concentrations, the inhibiting anions would be ineffective in preventing or delaying the onset of localized corrosion.

In this study, electrochemical tests were performed to determine the effect of electrolyte composition on the electrochemical behavior of Alloy 22, and its susceptibility to localized corrosion in SAW and SCW. The preliminary results presented here highlight the results of open circuit potential (OCP) measurements, as well as slow scan rate potentiodynamic polarization.

EXPERIMENTAL PROCEDURE

The material used in this study is Alloy 22. Its chemical composition and its yield and tensile strengths appear in Tables 2 and 3, respectively, as documented by the supplier. The composition is consistent with the ASTM B-574 standard [39]. The samples were supplied in the form of 25.4 cm long rods with a diameter of 0.625 cm. The samples were hand ground wet with 600-grit SiC paper (unless otherwise stated) and rinsed in distilled water before experimentation. A three-electrode cell with a capacity of 1000 cm^3 was used for experimentation. The volume of electrolyte in the cell was about 900 cm^3. A 2.54 cm length of the sample was immersed in the cell so that the total area of the sample in the electrolyte was ~5.38 cm^2. A silver/silver chloride (SSC) (Ag/AgCl) electrode was the reference electrode. The reference electrode was maintained near room temperature by mounting it at the end of a Luggin probe, which had a water jacket around it through which cold water was pumped to keep it cool. The temperature of the water in the cooling jacket was about 12°C. Thermal liquid junction calculations showed that potential variation caused by this phenomenon was in the order of mV (~10 mV maximum) for SAW and SCW. Also, according to MacDonald et al., a high KCl concentration in the reference electrode tends to suppress thermal liquid junction potentials across the boundary between the high and low temperature solutions [40]. The liquid junction potential variations were therefore ignored in further analyses at this stage of the work as they were thought to be negligible with regard to the short term open circuit potential and potentiodynamic polarization tests. The counter electrode was made of platinum (Pt) foil. Electrical connection was achieved through a piece of Pt wire spot welded to the foil. The temperature of the electrolyte was maintained by immersing the glass cell in a heating bath filled with silicon oil so that the level of the electrolyte in the cell was level with, or below the level of the silicon oil surrounding the cell. The sample was immersed in the cell after the electrolyte had attained the desired temperature. The temperature was monitored intermittently throughout the duration of the experiment with a thermocouple immersed in the cell. Electrochemical measurements were carried out using a potentiostat. The measurements included determinations at the open circuit potential (OCP), which was recorded for 24 hours (unless otherwise stated), and then potentiodynamic polarization (linear and cyclic) immediately afterwards. Pt foils with a total surface area of 4 cm^2 were used to measure the oxygen evolution potential (OEP). In this set of experiments, the open circuit potential was measured for 2 hours followed by linear potentiodynamic experiments. In all cases, the sweep rate was 0.1667 mV/s. The experiments were carried out in SAW and SCW at a temperature of 90°C unless otherwise stated. Their compositions and pH values appear in Table 1. The electrolytes were used under ambient aeration conditions, that is, in the as-prepared state with no gas (air, oxygen (O_2), Nitrogen (N_2), Argon (Ar) etc.) pumped through it before nor during the experiments. All electrolytes were prepared using certified American Chemical Society (ACS) grade chemicals.

Scanning electron microscopy (SEM) was carried out using a cold field emission scanning electron microscope to produce secondary electron (SE) images of sample surfaces. Acceleration voltages of 3 KV, 6 KV and 15 KV were used for imaging. Digital images were captured with a Quartz PCI / PC frame grabber. Qualitative and standardless quantitative energy dispersive X-ray microanalysis (EDX) of sample surfaces and deposits was performed using an Energy Dispersive X-ray Microanalysis system. It was equipped with a Si-Li X-ray detector behind an ultra-thin boron window working at a 15 KV acceleration voltage.

X-ray photoelectron spectroscopy (XPS) was carried out with a system equipped with a magnesium (Mg) X-ray source (Mg Kα 1253.5 eV). Spectra were recorded using a concentric hemispherical analyzer at the top of the chamber, giving an overall energy resolution of 1.1 eV. Survey scans (89.5 eV pass energy, 1 eV step size) and high-resolution XPS spectra (17.90 eV pass energy, 0.1 eV step size) were acquired to determine surface compositions. XPS has a detection sensitivity of 0.3 *atomic* percent or about 0.5 weight percent.

RESULTS

The Open Circuit Potential (OCP)

Table 4 shows the OCP of Alloy 22 in SAW and SCW, at ambient aeration, at 90°C after 24 hours. Some representative OCP transients are shown in Figure 2. There is a large scatter band in the values of OCP for Alloy 22 in SAW (Table 4 and Figure 2). The highest value recorded after a 24-hour period was 271 mV. The effect of the age of SCW on the OCP of Alloy 22 was investigated. SCW contains a high concentration of HCO_3^-, and as a result, it is affected by age as the decomposition or dissociation of bicarbonate (HCO_3^-) alters the pH of the electrolyte. This does not happen in SAW because it contains no HCO_3^- or any other specie that could readily dissociate under storage conditions. The pH of the 2-year-old SCW was 8.7, a difference of 0.7 units compared with the freshly prepared solution (Table 1). The OCP of Alloy 22 taken after a period of 24 hours in the fresh SCW is similar to its OCP in the 2-year-old SCW (Table 4). Figure 2 shows that the transients of Alloy 22 in these solutions of different ages are also similar.

Figure 3 shows the effects of the degree of aeration on the OCP of SAW. The highest OCP occurs under aerated conditions, followed by the ambient (Table 5), and then in the deaerated system. In the "aerated" mode, compressed natural air was pumped through the electrolyte throughout the experiment at a flow rate of 100 cc/minute, while in the "deaerated" mode; the electrolyte was purged with N_2 at the same flow rate. In both cases, the gas was pumped through the system for at least 1 hour before measurements commenced and throughout the duration of the experiments. Only two repeats were carried out in the aerated and deaerated environments.

Oxygen Evolution Potential (OEP)

Table 6 shows the oxygen (O_2) evolution potentials (OEP) measured on Pt electrodes in SAW and SCW, at ambient aeration, at 90°C, and for SAW at 60°C. As can be seen from representative polarization curves in Figure 4, the OEP (designated by the current density rise) is easily distinguishable from the passive current density. This facilitates an easy and fairly accurate measurement of the OEP. The OEP was measured as the point where the first visually noticeable permanent rise in current density from the passive current density was observed.

As expected from Pourbaix diagrams [41], the OEP reduces as pH increases. The OEP for SAW at 60°C and 90°C are similar (Table 6). In systems that contain Alloy 22, it will be assumed that in these electrolyte/temperature combinations, and above the appropriate listed potentials (Table 6), oxygen evolution will occur. Therefore any currents attributed to breakdown measured for Alloy 22 above these potentials under similar conditions would have a contribution from oxygen evolution.

Potentiodynamic Polarization

Figure 5a shows the cyclic polarization curves of Alloy 22 in SAW at 90°C. One curve measured after a high OCP was registered after 24 hours of immersion, and another curve taken after a moderate (close to the mean value) OCP was recorded. Figure 5a examines the effect of the OCP on the passive region and breakdown potential. Figure 5b shows polarization curves of Alloy 22 in SAW in aerated, deaerated and ambient conditions. Figure 5c shows cyclic polarization curves of Alloy 22 in SCW at 90°C. This graph shows one curve measured in fresh SCW while the other curve was in the 2 year old SCW. It examines the effect of the age of SCW on the behavior of Alloy 22.

Table 7 shows a summary of the breakdown potentials (E_E)[a] of Alloy 22 in SAW and SCW at 90°C. It includes the passive current density i_{pass} (taken at 0.5V (SSC)). This potential typically falls within the passive region of Alloy 22, whether in SAW or SCW (Figure 5). The breakdown potential was taken at a threshold value of $2x10^{-5}$ Acm^{-2}. At this current density, stable pitting or crevice corrosion would have commenced as evident from work carried out by various authors where pitting or crevice breakdown potentials were measured for various stainless steels, nickel and Alloy 22 [12,13,42,43]. The threshold values of 0.5V (SSC), and $2x10^{-5}$ Acm^{-2} are arbitrary values used as reference points as a basis for comparison of the data limited to those that are presented in this paper. They bear no other significance.

In Figure 5a, the curve that had a higher OCP after 24 hours of immersion posted the lower passive current density. There was no effect of the age (2 year old) of the electrolyte (SCW) on the behavior of Alloy 22 as shown in Figure 5c. Apart from the beginning of the polarization curves (up till about -0.05 V(SSC)), the two curves are virtually identical, and can be superimposed on each other. None of the cyclic polarization curves (Figures 5a and 5c) showed any hysteresis. A hysteresis loop would have been indicative of localized breakdown (pitting corrosion in this case, and crevice corrosion if breakdown occurred under an artificial crevice former, or in an occluded area on a sample [12, 13]). The polarization curves of Alloy 22 in SAW (Figure 5a) are much less complicated than those in SCW. In Figure 5a (SAW), once the current rise commenced from the passive current density, it continued until film breakdown whereas, in SCW (Figure 5c) there was a rise in current density at about 200 mV (SSC), which fell, and remained constant until about 730 mV before permanently rising. Alloy 22 showed two separate and distinct passive regions in SCW at 90°C (Figure 5c). From the data obtained from the Pt electrodes (Figure 4 and Table 6), which show that the mean OEP in the respective electrolytes occurred ~300 mV after the mean "breakdown potentials" of Alloy 22 (Table 7), coupled with the fact that there were no hysteresis loops visible in Figure 5a and 5c, transpassive dissolution of Cr appears to be the only mode of breakdown possible under these conditions on Alloy 22 in SAW and SCW at 90 °C. SEM and EDX data from Alloy 22 in SAW at 90 °C presented in Figure 6 support the notion of transpassive dissolution of Cr. Figure 6a shows the SEM image of the surface of the Alloy 22 sample, which was not exposed to SAW. Figure 6b shows the surface of the same sample after polarization in SAW at 90°C to 1.1 V(SSC). Craters or dimples caused by dissolution of the alloy can been seen on the surface of the sample. The dissolution was not localized, that is, it was not limited to specific areas of the metal surface, but took place throughout the entire area exposed. The remnant of the dissolution product (with the mud-crack morphology) removed after the experiment from the area exposed to electrolyte and polarized can be seen at the bottom of some of these craters. The dissolution product is easily washed off the sample with water immediately it is removed from the cell after experimentation, but becomes more adhesive to the surface after it has dried. At higher magnification of the area shown in Figure 6b, grain boundaries are visible (Figure 6c), and present further evidence of dissolution. Again, dissolution products are visible at the bottom of some of the depressions. A photo of the dried dissolution product is presented in Figure 6d, which clearly shows the mud-crack morphology of the deposit upon drying. Figures 6e and 6f show qualitative EDX spectra of the unexposed metal surface (Figure 6e) and that of the deposit (Figure 6f). The intensity of the peaks of the deposit of the dissolution product when compared to that of the metal surface not exposed to electrolyte show a depletion of Ni, accompanied by an increase in intensity of the Mo, W and Cr peaks, all of which are consistent with transpassive dissolution. It should be noted however that the Mo peak is likely to be a composite (overlapping peaks) of Mo and S peaks, while that of W is a composite of W and Si peaks. Therefore, the peak intensities shown by Mo and W cannot be entirely attributed to these elements. More detailed analyses are required on the samples from SAW exposure, as well as on those from SCW

[a] "Breakdown potentials" as employed here is used to denote the potential(s) at which any type of breakdown of the passive *film* whether localized (e.g., pitting or crevice), or due to general dissolution, or transpassive dissolution of chromium or molybdenum occurs.

exposure to resolve this. The dissolution products that formed on Alloy 22 in SCW were opaque (very light yellow color tending towards white), while those that formed of Alloy 22 in SAW were golden brown. In SAW at a temperature of 90 °C, Alloy 22 broke down (transpassively) at about 0.664V(SSC) (Table 6). The potential at which the sample of Alloy 22 was polarized to (1.1 V(SSC)) was about 155 mV (SSC) above the OEP as measured on Pt (Table 6), and about 436mV above the transpassive potential as measure on Alloy 22 in SAW (Table 7). This means that at a sweep rate of 0.1667 mV/s, transpassive dissolution would have taken place for an estimated time period of 2777 s (~0.77 hours). Neither the value of the OCP (Figure 5), nor the degree of aeration (Figure 6) in SAW affected the transpassive potential.

The anodic peak (hump) in the polarization curve of Alloy 22 in SCW in Figure 5c (which started at about 200 mV (SSC)) appears to be due to the transformation of molybdenum from Mo (IV) to Mo (VI). It should be noted that the point at which the current density attained the threshold value of 2 x 10^{-5} Acm^{-2} fell within the up-rise of the hump (at about 254-277 mV (SSC), (Table 6). The passive region after the hump typically possessed a current density higher than the threshold value of 2 x 10^{-5} Acm^{-2}, and by the break down criterion set forth earlier, the sample would be adjudged to have broken down. Although the current density in this second passive phase is high (5 – 7 x10^{-5} Acm^{-2} at 0.5 V(SSC); Table 7), Alloy 22 seemed to exhibit some degree of passive stability in this region up till over 700 mV (SSC). XPS data taken in the regions immediately before (125 mV) and after (375 mV and above) the hump showed that the metal surface consisted predominantly of a Cr/nickel (Ni) rich oxide film (Figure 7). Figures 7a to 7d show the oxidation states of Mo, Ni, Cr and O at various potentials. 125 mV corresponds to a region immediately before the anodic peak, while 375 mV and above represent regions immediately after the anodic peak (Figure 5c). It can be seen from these spectra that Mo changed from the IV to the VI oxidation state (Figure 7a). There was no change in the spectra of Cr (Figure 7c), neither were there any significant shifts in the spectra of Ni and O (Figure 7b and 7d).

DISCUSSION

It is important to know the OCP and breakdown potential (if any) that Alloy 22 will register under service conditions in Yucca Mountain, and any factors that might affect the final value of the OCP under these conditions so as to accurately estimate the region of passivity, and thus the possible region of kinetic immunity of the alloy. It is imperative that the rest potential or OCP of the alloy stays within the passive region under any possible repository conditions in order to guarantee kinetic immunity throughout the projected service life of the waste containers in Yucca Mountain. It is quite clear that the electrolyte compositions, coupled with the degree of aeration (Figures 2 and 3; Tables 4 and 5) are important factors as shown with regard to the OCP. The pertinent questions when considering the relationship between the OCP and any possible breakdown potential include whether the OCP will rise or fall over time, what may cause the rise or fall in OCP, whether these changes are reversible, and how any of these changes might affect the value of the breakdown potential of Alloy 22 (if the possibility of breakdown occurring exists). The asymptotic nature of the curves for the OCP of SAW and SCW in Figures 2 and 3 suggest that the OCP might rise over time, and raises question as to how long experiments must be carried out to determine the final steady state value of the OCP. Twenty four-hour measurements like the ones presented in Figures 2 and 3 are hardly the type of measurements to be used to predict what might happen over geological periods of time. However, on-going long-term corrosion tests at our laboratory suggest that a rise in OCP might occur with time. However, the extent to which the OCP will rise, to what extent dissolved species in the electrolyte and any scales or deposits that might form on the sample surfaces may affect this rise in OCP, whether these observed increases in OCP are reversible, and how all these factors might affect any possible breakdown (i.e., whether the OCP will ever rise to the potential of breakdown) are yet to be determined. If present, the role of any scale

formation on the samples must also be clearly separated from any changes due to any transformations in the oxide film. These will be addressed in future publications.

The high OCP value of Alloy 22 obtained from two of the six repeats in SAW (268 and 271 mV) cannot be conclusively explained from the data collected so far. More experiments are required in this area to fully understand the reason(s) for the high OCP. Nevertheless, one reason for the high OCP obtained might be due to oxide film effects. The samples were hand-ground with 600-grit SiC paper as opposed to the use of a mechanical grinding wheel. The lower passive current density obtained on Alloy 22 in SAW (Figure 5a) for the sample with the high OCP compared with the sample with the more moderate OCP is consistent with a situation where the sample with the higher OCP had a better (probably with fewer defects) oxide film. Earlier work performed by Kehler et al. [13] found a strong dependence of the age of the oxide film on the behavior of Alloy 22. Kehler et al. found that the open circuit potential of freshly polished Alloy 22 and Alloy 625 samples posted more negative values compared with laboratory air-aged samples. The fresh Alloy 22 samples had a mean OCP value of about 200 mV less than the air aged ones while those of Alloy 625 had OCP values that were about 75 to 100 mV lower when freshly ground. Also, they found that the crevice stabilization potentials for Alloy 22 were higher for the air-aged samples compared with the freshly ground samples, furthermore, the crevice stabilization potential of Alloy 625 did not seem to be as sensitive to oxide film age. For instance, their cumulative probability plots showed that at a 50% probability that crevice stabilization will occur in their 100:1 electrolyte (5 M lithium chloride (LiCl):0.05 M [SO_4^{2-} + NO_3^-]), the difference in potential between the freshly polished and aged samples approached 200 mV for Alloy 22 and was less than 50 mV for Alloy 625. They speculatively attributed the difference in crevice stabilization potential either to differences in the oxide film thickness or to the amount of defects present in the oxide film of the freshly polished samples. Although it is difficult to see how the ground waters (Table 1) that might be present at Yucca Mountain could evolve into the relatively aggressive electrolytes used by Kehler et al., what their work showed was that differences in oxide film age are evident when the bounds of localized corrosion resistance of Alloy 22 were probed. With benign electrolytes like SAW and SCW (compared with what Kehler et al. used), the bounds of localized corrosion resistance could not be probed. The result as seen in Figures 5a, 5c and 6 is transpassive dissolution.

The fact that the specimens in aerated SAW exhibited higher OCP values (on average) compared with the ambient and deaerated systems is not surprising (Figure 3, Table 5), neither is the fact that the degree of aeration did not affect the transpassive potential (Figure 5b). However, what is clear from this short-term data is that the amount of dissolved oxygen or the degree of aeration that will be present under repository conditions is of importance in order to reasonably estimate what the highest OCP under operating conditions is likely to be. It is likely that upon long-term exposures, all the curves in Figure 3 would converge to a single value. For modeling purposes, the most conservative OCP values (highest values) must be used, and these will be achieved faster in aerated electrolytes. Studies carried out in aerated electrolytes also seem to be the most reasonable approach to take since under repository condition, after the initial dry period (due to higher temperatures), one might assume that only a thin film of ground water will exist on the canister surfaces once the ground water starts to drip on them, and that these thin films of water will have a lot of dissolved oxygen in them compared with bulk solutions. It will be prudent to take other issues such as how the formation of scales (such as silicates), and the presence of other oxidants such as H_2O_2 might affect the OCP into consideration. It is also significant that the behavior of Alloy 22 did not change with the age of SCW, which is susceptible to pH variations from the dissociation, or decomposition of HCO_3^-. This is significant because it is thought that upon concentration through the cyclic wetting and dying process expected in Yucca Mountain, the composition of the resulting J-13 concentrate will be closest to that of SCW (rather than that of SAW). This might suggest that the possibilities of the electrochemical behavior of Alloy 22 being affected by variations caused by a change in ground water are reduced.

The lack of hysteresis loops in Figures 5a and 5c suggest that Alloy 22 is not susceptible to pitting corrosion in neither SAW nor SCW at 90°C. Rather, Alloy 22 is only susceptible to transpassive dissolution of Cr at elevated potentials (e.g. above 0.6V(SSC) in SAW) in these electrolytes. Experiments are ongoing to determine the susceptibility of Alloy 22 to crevice corrosion in SAW and SCW. The significance of these results is that failure through the nucleation and stabilization of damaging pits on a non-occluded surface area of a nuclear waste canisters devoid of any scales or deposits at temperatures not greater than 90°C would be very difficult, provided the concentration of the ground waters never get more concentrated or aggressive than SAW and SCW. It has not been determined whether Alloy 22 becomes susceptible to pitting corrosion in these electrolytes at higher temperatures (100-120°C). Under service conditions, transpassivity will only occur if the OCP equals or exceeds the transpassive potential. However, a pertinent question to consider is whether the transpassive potential is attainable under the proposed geological repository conditions. This question still needs to be answered conclusively with experimental data. Nonetheless, the high field strength required to generate the magnitude of charge needed to bring this conditions ($\sim 10^6$ Vcm^{-1}) might be difficult to attain. Thus far, OCP values from the long-term corrosion facility being monitored in our laboratory have not conclusively shown that the transpassive potential could be possibly attained under free corrosion conditions.

The transformation of Mo from the IV to the VI valence state occurs at a lower potential (as observed from XPS spectra in Figure 7) compared with the transpassivation of Cr. The oxidation of Mo (IV) to Mo (VI) is represented by the anodic peak (hump), which starts at about 200 mV (SSC) in Figure 5c. This transformation is pH sensitive, because it was not observed at the lower pH value of SAW (2.78). A similar behavior has been observed on Alloy C-276 in 1% NaCl at a temperature of 100°C by Postlethwaite et al. [10] which they attributed to the transpassivity (oxidation) of Mo. Again, long-term corrosion data needs to be gathered to explore any possibility of the oxidation of Mo (from (IV) to (VI)) occurring under free corrosion conditions after long periods of time. What is clear is that in the mid to high range pH solutions, the oxidation of Mo is attainable at a lower potential compared with that of Cr.

The presence of the second passive region after the anodic peak due to the oxidation of Mo suggests that Alloy 22 still maintains some degree of passivity in SCW, under the conditions tested (Figure 5c). However, if one were to assume such current density values (as obtained in this second passive region), it might indicate an unacceptably high dissolution rate over geological periods for the metal on the waste package. The tenacity of this second passive region to dissolution is therefore questionable and at best uncertain. Again, the possibility of this occurring under free corrosion conditions is remote due to the field strength required to maintain such high current densities. It must be noted that data shown in Figure 5 are from short-term potentiodynamic experiments, and potentiostatic tests might better explain the evolution of current density with time.

CONCLUSIONS

- Alloy 22 is not susceptible to localized breakdown due to pitting corrosion in SAW or SCW at 90 °C.
- Transpassive dissolution of Alloy 22 in SAW and SCW can occur under highly oxidizing conditions.
- Under the experimental conditions (24 hr OCP exposures at 90 °C) tested in SAW, the value of the OCP does not affect the potential at which transpassivity commences on Alloy 22.
- Up to a period of 2 years, the age of SCW solution does not affect the electrochemical behavior of Alloy 22.

REFERENCES

1. Civilian Radioactive Waste Management (CRWMS) Management and Operating Contractor (M&O), Licensing Application Design Selection (LADS) Report, B00000000-01717-4606-00123 Rev. 01 ICN 01, CRWMS M&O, Las Vegas, 1999.
2. J. Harrar, J. Carley, W. Isherwood and E. Rabeer, in Report of the Committee to Review The Use of J-13 Well-water in the Nevada Nuclear Waste Storage Investigations, UCID-21876, Lawrence Livermore National Laboratory, January 1990.
3. Wang, G.E. Gdowski, J. Estill, S. Gordon, S. Doughty, K. King and D. McCright, Corrosion'98, 1998 Paper No. 161.
4. N.D. Rosenberg, G.E. Gdowski, and K. G. Knauss, Applied Geochemistry, 2001. **16**: p.1231.
5. K.A. Gruss, G.A. Cragnolio, D.S. Dunn and N.Sridhar, Corrosion '98, 1998, Paper No. 149.
6. S.J. Lukezich, The Corrosion Behavior of Ni-Base High Performance Alloys in Simulated Repository Environments, MS Thesis, The Ohio State University 1989.
7. M. H. Wilde, and D.E. Wilde, Corrosion Science, 1993. **34**: p. 433.
8. D.W. Shoesmith, B.M. Ikeda, F. King, and S. Sunder, in, Prediction of Long Term Behavior for Radioactive Nuclear Waste Disposal, Proceedings of the CORROSION/96 Research Topical Symposia," Sponsored by the NACE Research Committee, 1996, p.101.
9. A. Asphahani, patent Number 4,533,414.
10. J. Postlethwaite, R.J. Scoular , and M.H. Dobbin,. Corrosion, 1988. **44**(4): p. 199.
11. G.A. Cragnolino and N. Sridhar. Corrosion, 1991. **47**(6): p. 465.
12. B. A. Kehler, G.O. Ilevbare and J.R. Scully Corrosion 2000, Paper No. 00182
13. B. A. Kehler, G.O. Ilevbare and J.R. Scully Corrosion 2001, Paper No. 01141
14. B. A. Kehler, G.O. Ilevbare and J.R. Scully Corrosion 2001, Crevice Corrosion Behavior, of Ni-Cr-Mo Alloys: Comparison of Alloys 625 and 22, NACE Topical Research Symposium, March 2001, p.30.
15. S.J. Mulford and D. Tromans, *Crevice Corrosion of Nickel-Based Alloys in Neutral Chloride and Thiosulfate Solutions.* Corrosion, 1988. **44**(12): p. 891.
16. R.S. Lillard, M.P. Jurinski, and J.R. Scully, *Crevice Corrosion of Alloy 625 in Chlorinated ASTM Artificial Ocean Water.* Corrosion, 1994. **50**(4): p. 251.
17. E.L. Hibner, Corrosion'86, 1986, Paper No. 181.
18. E. L. Hibner, Materials Performance, 1987. **26**(3): p. 37.
19. K.A. Gruss, G.A. Cragnolino, D.S. Dunn and N. Shridhar, *Repassivation Potential for Localized Corrosion of Alloys 625 and C22 in Simulated Repository Environments*, 1998, U.S. Nuclear Regulatory Commission (Washington, D.C.) and Center for Nuclear Waste Regulatory Analyses, Southwest Research Institute (San Antonio, TX),
20. D.S. Dunn, G.A. Cragnolino, and N. Sridhar, Corrosion, 2000. **56**(1): p. 90
21. N. Sridhar and G.A. Cragnolino, *Applicability of Repassivation Potential for Long-Term Prediction of Localized Corrosion of Alloy 825 and Type 316L Stainless Steel.* Corrosion, 1993. **49**(11): p. 885.
22. G.A. Cragnolino, *Assessment of Localized Corrosion of Alloys 825, 625, and C-22 for HLW Containers*, 1998, Waste Package Degradation Expert Elicitation Workshop
23. H.P. Hack, Materials Perfomance, 1983. **22**, (6): p.24.
24. G.E. Gdowski Survey of Degradation Modes of Four Ni-Cr-Mo Alloys UCRL-ID-108330, 1991. p.30-31.
25. Haynes International, Inc., Product Brochure H-200B, Haynes international Inc. Kokomo, IN, 1987. p.15.
26. Haynes International, Inc., Product Brochure H-2019C, Haynes international Inc. Kokomo, IN, 1988. p.22.

27. J. C. Farmer, D. McCright, G.E. Gdowski, F. Fang, T. Summers, P. Bedrossian, J. Horn, T. Lian, J. Estill, A. Lingenfelter, and W. Halsey, General and Localized Corrosion of Outer Barrier of High-Level Waste Container in Yucca Mountain, May 2000. Preprint UCRL-JC-138890, Lawrence Livermore National Laboratory, Technical Information Department Digital Library.
28. H.H Uhlig and J.R. Gilman, Corrosion, 1964. **20**: p.289t.
29. H. P. Leckie and H.H. Uhlig, J. Electrochem. Soc., 1966. **117**: p. 1152.
30. I.L. Rozenfeld, and I.S Danilov, Corrosion Science, 1967. **7**: p.129.
31. E.A. Lizlovs and A.P. Bond, J. Electrochem Soc., 1969. **116**: p.574.
32. Z. Szklarska-Smialowska, Corrosion Science, 1971. **11**: p.209.
33. Z. Ahmed, Corrosion, 1977. **33**: p.161.
34. H.H. Strehblow, and B. Titze, Corrosion Science, 1977. **17**: p.461.
35. H.C. Man and D. R. Gabe, Corrosion Science, 1981. **21**: p.713.
36. R.C. Newman and T Shahrabi, Corrosion Science, 1987. **27**: p.827.
37. H. Yashiro and K. Tanno, Corrosion Science, 1990. **31**: p. 485.
38. P.C. Pistorius, and G.T Burstein, Corrosion Science, 1992. **33**: p.1885.
39. ASTM B574, Annual Book of ASTM Standards, Nonferrous Metal Products, 2000. Volume 02.04, p.531,. American Society of Testing and Materials, West Conshohocken, PA.
40. D.D. MacDonald, A.C Scott, and P. Wentrcek, J. Electrochem. Soc., 1978. **126**: p.908.
41. M. Pourbaix, in Atlas of Electrochemical Equilibria in Aqueous Solutions, 1974. p.97. National Association of Corrosion Engineers, Houston TX.).
42. M, Karaminezhaad-Ranjbar, J. Mankowski, and D.D. MacDonald, Corrosion, 1985. **41**: p.197.
43. H. Guyader, V. Debout, and A.M. Grolleau, Crevice Corrosion of Ni base alloys and Highly Alloyed Stainless Steels in Sea Water in EUROCORR '99 Proceedings [EUROCORR '99 Proceedings], Sept. 1999. Event No. 227, p. 200. DECHEMA, Chemische Technik und Biotechnologie e.V., Frankfurt am Main, Germany.

ACKNOWLEDGEMENTS

The Department of Energy Office of Civilian Radioactive Waste Management (OCRWM) sponsored this work. This work was done under the auspices of the U.S. Department of Energy (DOE) by the University of California, Lawrence Livermore National Laboratory (LLNL) under Contract No. W-7405-Eng-48. This work is supported by Yucca Mountain Site Characterization Project, LLNL. Contributing researchers include John Estill, Steve Gordon, Kenneth Evans, Gary Hust, Shirley Evans, Peter Bedrossian and James (Jim) Ferreira. Technical comments by Daniel McCright and Raul B. Rebak.

Table 1. Chemical composition (in mg/l) of simulated ground waters used as electrolytes. These electrolytes are based upon the J-13 well water.

Ion	SCW pH 8	SAW pH 2.8	J-13 pH 7.4
K^+	3400	3400	5.04
Na^+	40,900	40,900	45.8
Mg^{2+}	< 1	1000	2.01
Ca^{2+}	< 1	1000	13.0
F^-	1400	0	2.18
Cl^-	6700	24,250	7.14
NO_3^-	6400	23,000	8.78
SO_4^{2-}	16,700	38,600	18.4
HCO_3^-	70,000	0	128.9
SiO_3^{2-}/Si	~ 40	~ 40	61

SCW: Simulated Concentrated Water. SAW: Simulated Acidified Water. J-13: Water from well near proposed repository site.

Table 2. Chemical composition of Alloy 22 (UNS No. N06022) given in weight percent.

Element	Actual Composition	ASTM Requirements (ASTM B576)	
		Minimum	Maximum
Mo	13.1	12.5	14.5
Cr	22.3	20.0	22.5
Fe	3.4	2.0	6.0
W	2.9	2.5	3.5
Co	0.8	0.0	2.5
C	0.004	0.000	0.015
Si	0.06	0.00	0.08
Mn	0.29	0.00	050
V	0.15	0.00	0.35
P	0.01	0.00	0.02
S	<0.01	0.00	0.02
Ni	Balance	Balance	Balance

Table 3. Tensile and yield strengths (in PSI) of Alloy 22 (UNS No. N06022).

	Tensile Strength	Yield Strength (0.2%)	Elongation (in 4D*)
ASTM Requirements	100,000	45,000	45.0%
Actual	135,430	87,560	47%

*4D = 4 times the diameter

Table 4. OCP (vs. SSC) of Alloy 22 in SAW and SCW, at ambient aeration, at 90°C after 24 hours..

Electrolyte	OCP (Lowest value)	OCP (Highest value)	OCP (Mean)	Number of repeats
SAW	-0.116	0.271	0.066±0.177	6
SCW (Fresh Electrolyte)	-0.148	-0.114	-0.129±0.014	6
SCW (2 yr Old Electrolyte)	-0.202	-0.129	-0.168±0.054	4

All error values are correct to a 95% confidence level

Table 5. OCP (vs. SSC) results obtained from other modes of aeration in SAW at 90°C.

Electrolyte	OCP(1)	OCP(2)	OCP (Mean)*
Aerated	-0.0302	-0.0218	-0.0260
Deaerated (Purged with N_2)	-0.2992	-0.3034	-0.3013

*Only two repeats were carried out in these modes of aeration.

Table 6. Oxygen evolution potentials (OEP) measured (vs. SSC) on Pt electrodes in SAW and SCW, at ambient aeration, at 90°C.

Electrolyte	OEP (Lowest value)	OEP (Highest value)	OEP (Mean)	Number of repeats
SAW at 90°C	0.884	0.976	0.945±0.026	8
SCW at 90°C	0.535	0.618	0.571±0.023	8
SAW at 60°C	0.894	0.935	0.933±0.017	8

All error values are correct to a 95% Confidence level.

Table 7. Breakdown potentials and passive current densities of Alloy 22 measured in SAW and SCW at 90°C in undeaerted solutions. The breakdown potential E_E is the potential at which the current density of $2x10^{-5}$ Acm^{-2} is attained. Passive current density i_{pass} is the current density measured at 0.5V(SSC).

Electrolyte	E_E (Lowest)	E_E(Highest)	E_E (Mean)	i_{pass}(Mean)	Number of repeats
SAW	0.661	0.666	0.664±0.002	$2.517±1.974e^{-6}$	6
SCW (Fresh)	0.254	0.277	0.268±0.009	$7.005±1.358e^{-5}$	6
SCW (2 yr old)	0.253	0.256	0.255±0.002	$5.350±1.933e^{-5}$	4

All error values are correct to a 95% Confidence level. All E_E values are measured in volts (V) against the SSC. All current densities are measures in Acm^{-2}.

a.

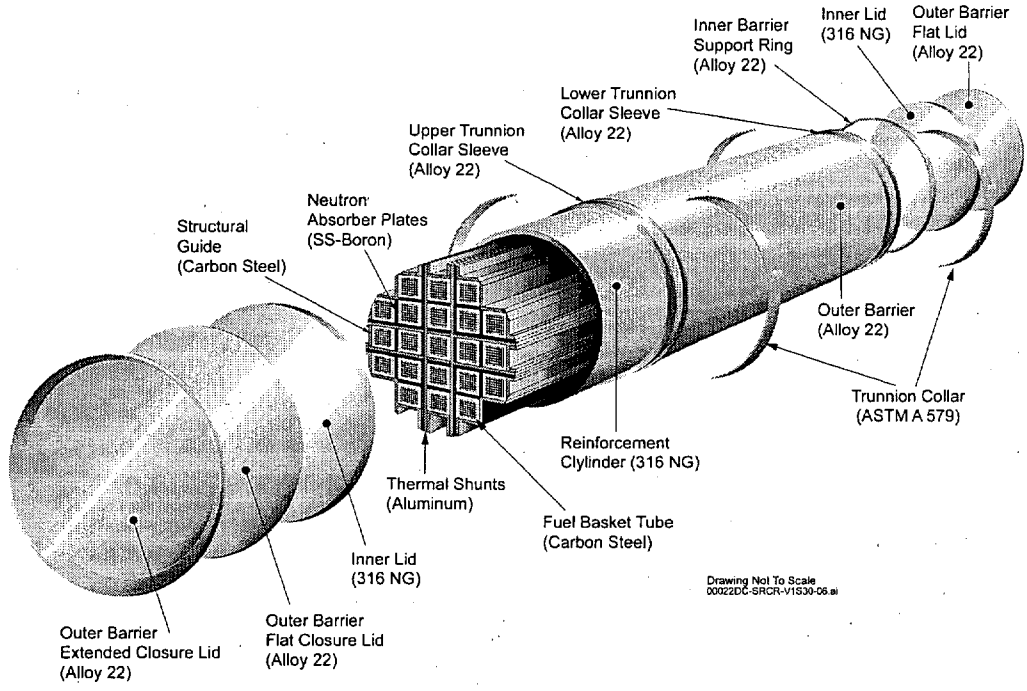

b.

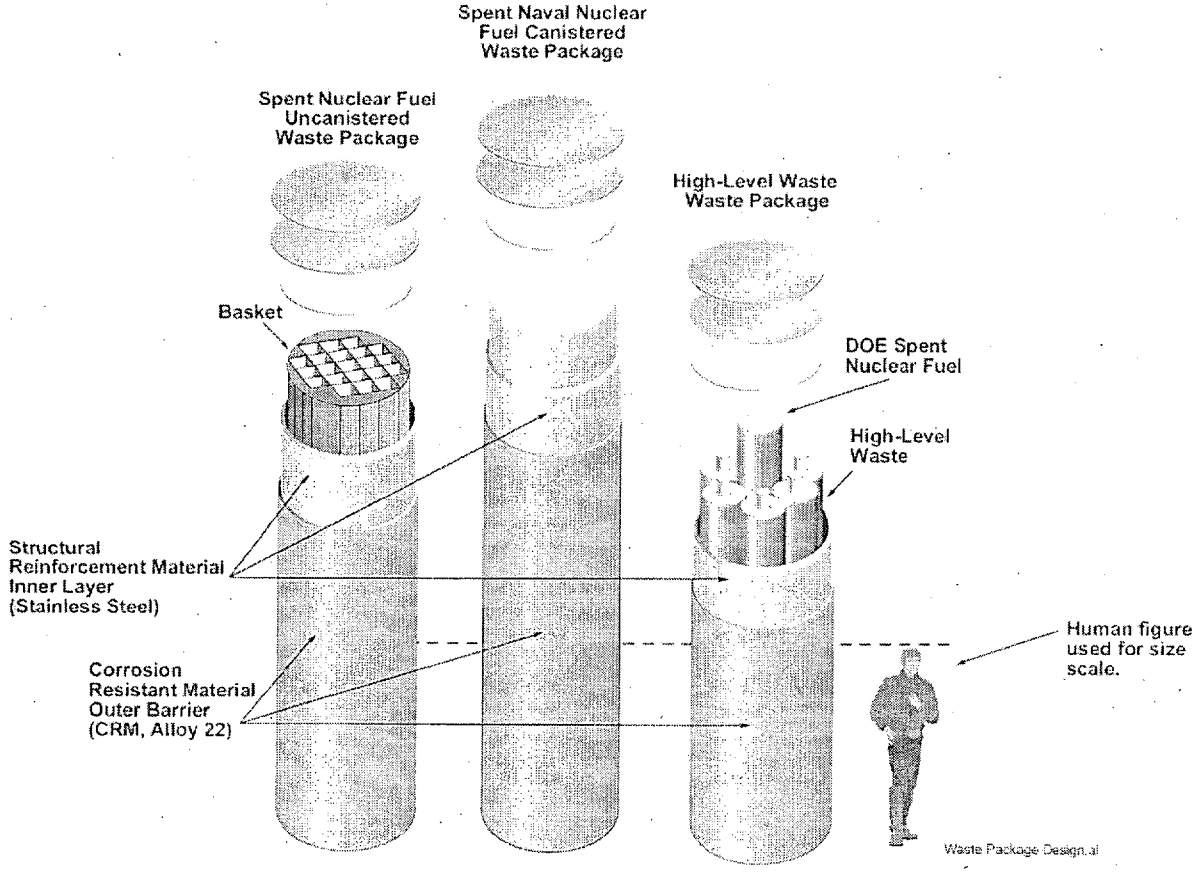

Figure 1. Representative waste package designs

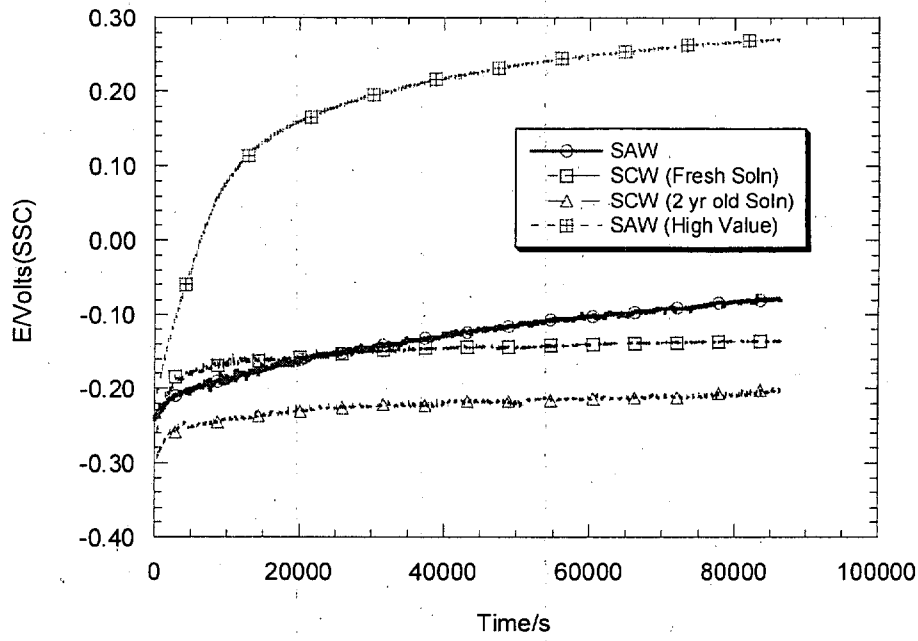

Figure 2. OCP of SAW and SCW on Alloy 22 at 90°C for 24 hours in ambient solution.

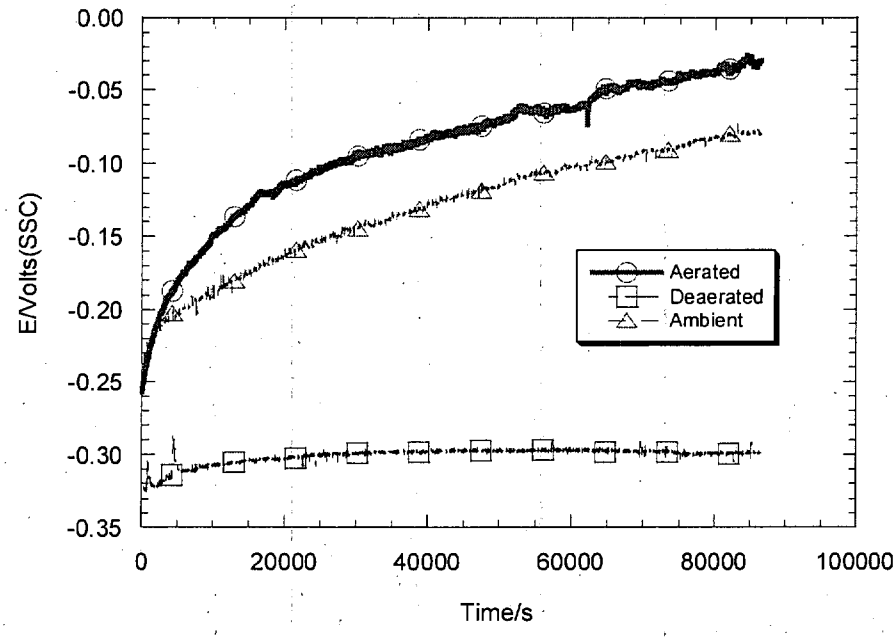

Figure 3. OCP of Alloy 22 in SAW under different aeration conditions.

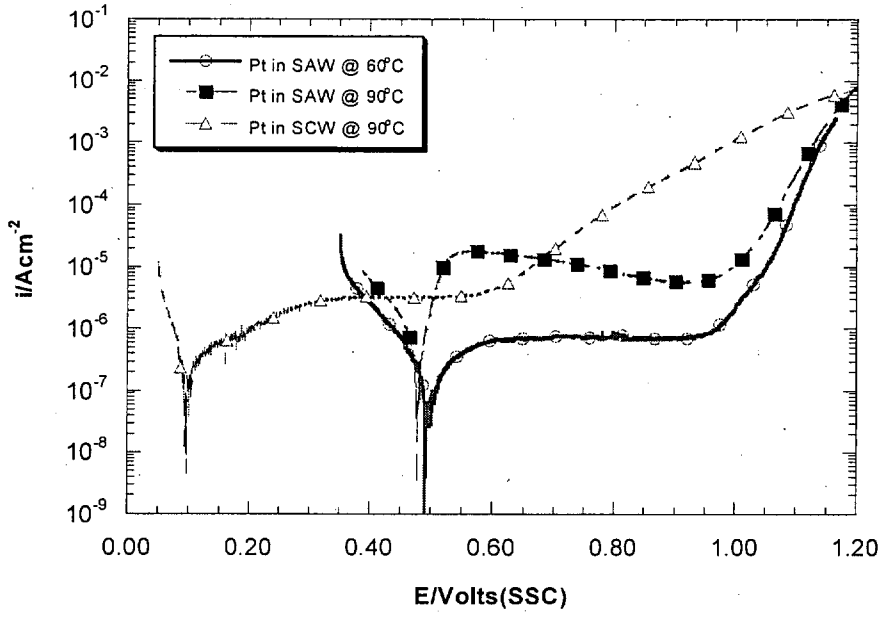

Figure 4. Platinum in SAW and SCW at 60 °C and 90°C. Sweep rate was 0.1667 mV

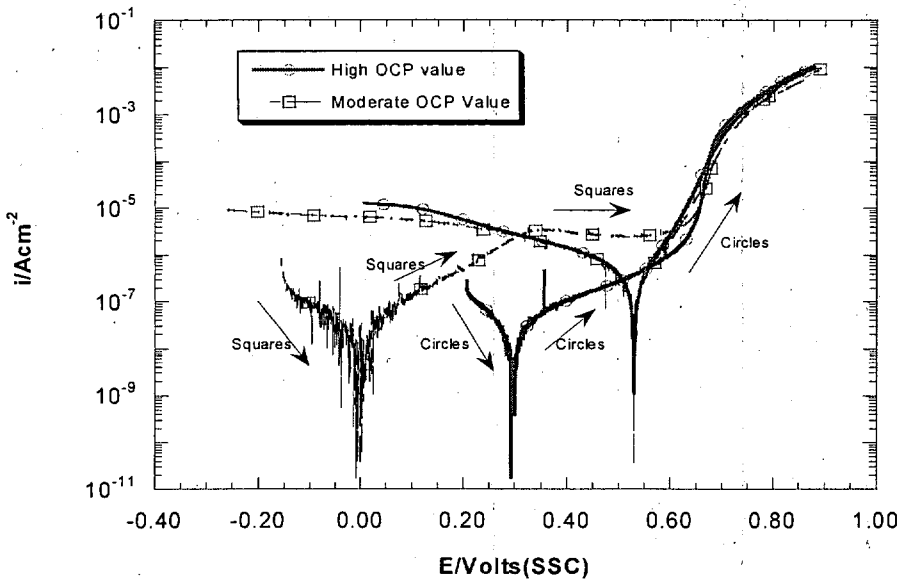

Figure 5a. Cyclic polarization curves of Alloy 22 in SAW at 90°C. This graph shows one curve measured after a high OCP was registered after 24 hour of immersion, and another curve taken after a moderate (close to the mean values) OCP was recorded after 24 hours. Sweep rate for the forward and reverse sweeps was 0.1667 mV/s. Surface finish: 600-grit SiC paper. Surface Area: 5.38cm^2.

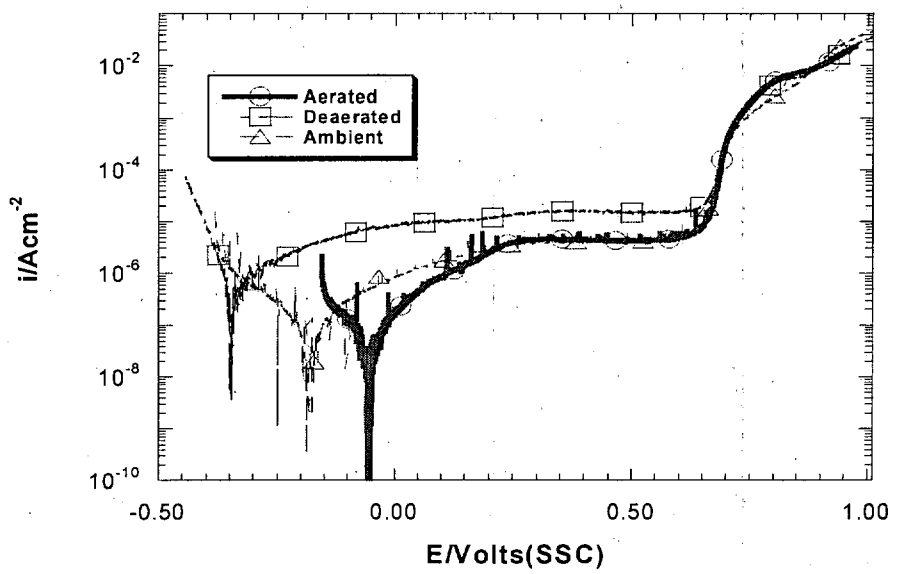

Figure 5b. Polarization curves of Alloy 22 in SAW at different aeration levels at 90°C. This graph shows that Alloy 22 dissolves transpassively at a similar potential irrespective of the degree of aeration. Sweep rate for the forward and reverse sweeps was 0.1667 mV/s. Surface finish: 600-grit SiC paper. Surface Area: 5.38cm^2.

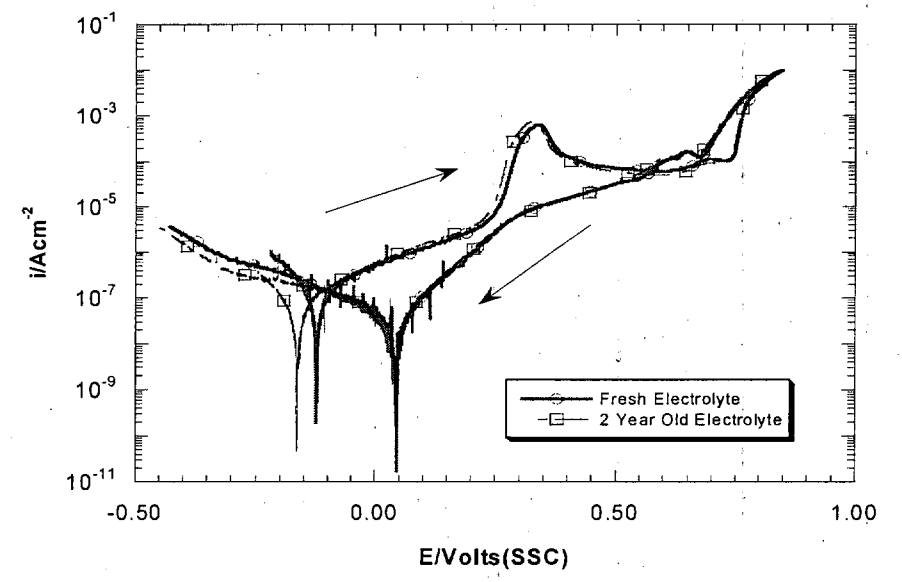

Figure 5c. Cyclic polarization curves of Alloy 22 in SCW at 90°C. This graph shows one curve measured in fresh SCW while the other curve was taken in 2 year old SCW. Sweep rate for the forward and reverse sweeps was 0.1667 mV/s. Surface finish: 600-grit SiC paper. Surface Area: 5.38cm^2.

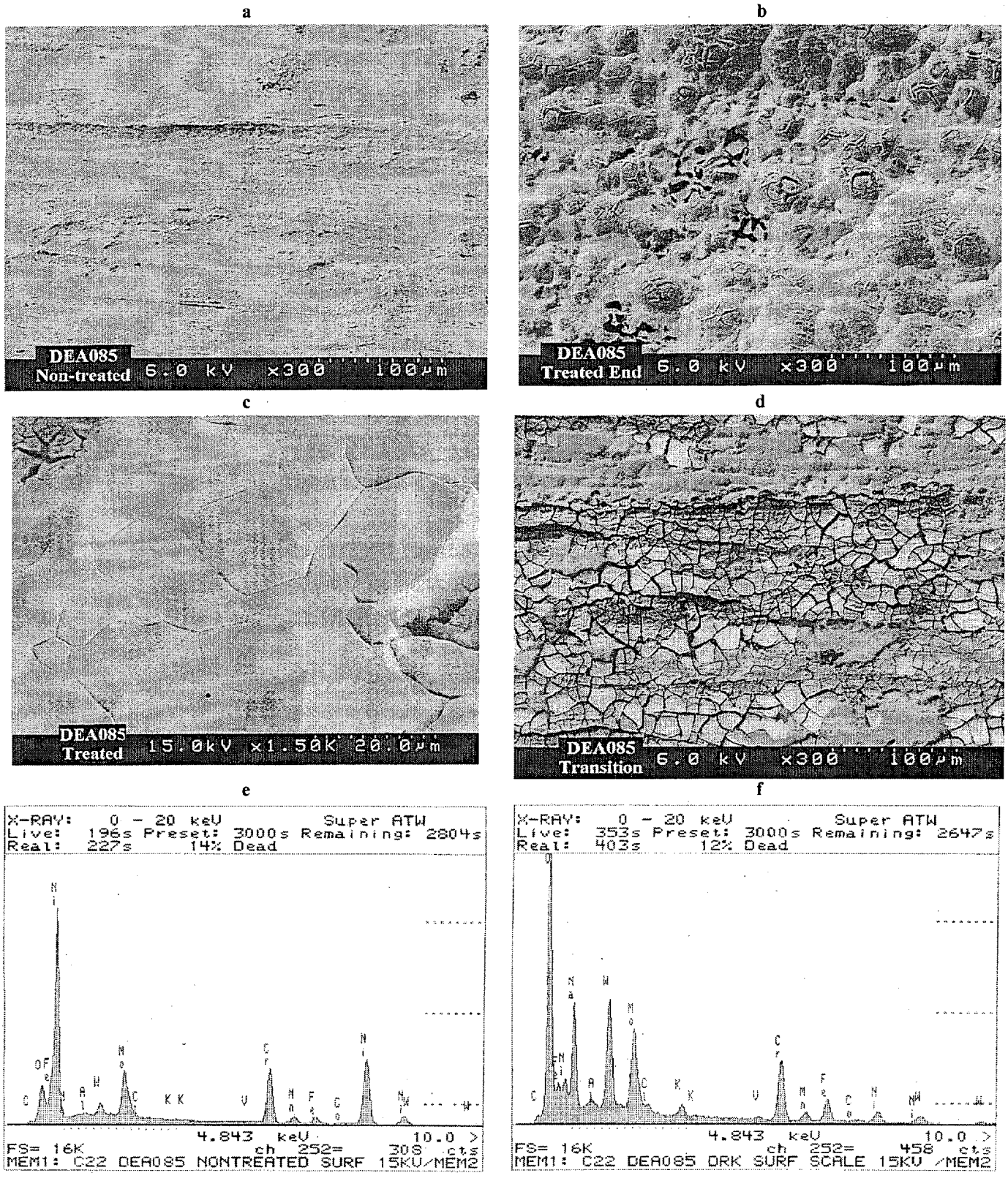

Figure 6. (a) SEM image of an Alloy 22 surface not exposed to electrolyte (magnification: x300); (b) surface after polarization in SAW at 90°C to 1.1V (SSC) (magnification: x300); (c) surface after polarization in SAW at 90°C to 1.1V (SSC) (magnification: x1500); (d) dissolution product from Alloy 22 deposited on metal surface after polarization in SAW at 90°C to 1.1V (SSC) (magnification: x300); (e) EDX spectrum taken from sample surface not exposed to electrolyte; (f) EDX spectrum taken from sample surface after polarization in SAW at 90°C to 1.1V (SSC).

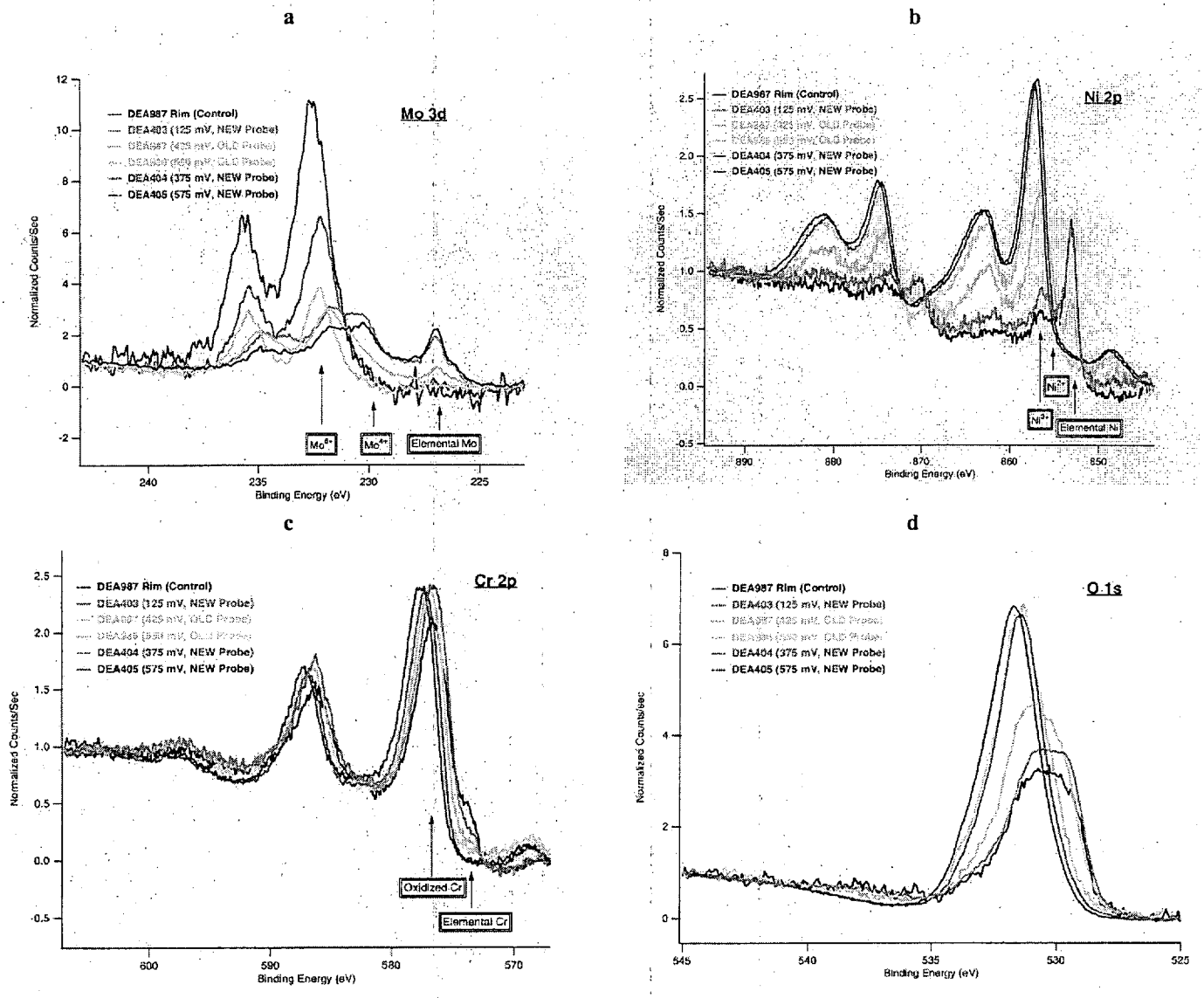

Figure 7. XPS spectra taken at for Alloy 22 in SCW.